



## PVA/cellulose nanocrystal nanocomposites films incorporated with copper nanoparticles; characterization and antibacterial performance

Ahmed El-Gendy, Mohamed A. Diab, Ragab E. Abou-Zeid, Ahmed K. Saleh\*



CrossMark

Cellulose and Paper Department, National Research Centre, 33 El-Bohouth St., Dokki, P.O. 12622, Giza, Egypt

### Abstract

Due to their unique structure and properties, biocompatibility, adaptable surface chemistry, optical transparency, non-toxic, biodegradability, and improved mechanical properties, cellulose nanocrystals (CNCs) are considered very promising for use as reinforcement material in construction of high-performance nanocomposites. Many biodegradable polymers are used as a matrix in the manufacture of these nanocomposites, among them polyvinyl alcohol (PVA). In the current study, the nanocomposites films, PVA loaded by CNCs prepared from rice husk and PVA loaded by CNCs and copper nanoparticles (Cu-NPs) were fabricated. The prepared nanocomposite films were characterized by scanning electron microscopy (SEM), X-ray diffraction (XRD), thermogravimetric analysis (TGA&DTA), and mechanical properties. The prepared nanocomposites films were evaluated for their antibacterial activity by disk diffusion technique against pathogenic bacteria. The results reveal that PVA films loaded by CNCs and Cu-NPs have improved tensile strength as well as efficient antibacterial activity against Gram-negative and Gram-positive strains and are promising to be used as packaging material.

**Keywords:** Cellulose nanocrystals, copper nanoparticles, PVA/CNCs/Cu-NPs nanocomposites, Antibacterial activity

### 1. Introduction

Lignocellulosic biomass is widely considered one of the best renewable resources on earth. In addition to this, it is widespread across the globe, with large quantities in numerous areas [1]. In today's agricultural industry, rice husk makes up one of the largest waste products. Rice husks are the hard coverings of rice grains, which are separated from the grains during milling and agricultural biomass production. Organic wastes make up to 20% of rice's weight and comprise of cellulose (50%), lignin (25%–30%), silica (15%–20%), and moisture (10%–15%). Since it contains a high amount of cellulose and can be chemically altered, it makes CNC extraction possible [2]. CNCs are needle-like in shape and smaller than 100 nm in length with high degrees of crystallinity [3]. Besides their large surface area,

high mechanical strength, and high aspect ratio, CNCs are hydrophilic, non-toxic, low bulk density, biocompatible, and also biodegradable [4, 5]. Considering the high strength and stiffness of CNCs produced from different natural sources, combined with their low weight, biodegradability, and environmental advantages, CNCs are emerging as a new class of renewable nanomaterials [6-8].

CNCs have specific characteristics that make them ideal reinforcements for high-performance nanocomposites that exhibit sustainability. For paper coating and textile sizing applications, PVA acts as a matrix, mimicking the properties of natural polymers [9, 10], and can be crosslinked with CNCs as shown in figure 1. This type of polymer is widely applied for the production of films in various industrial

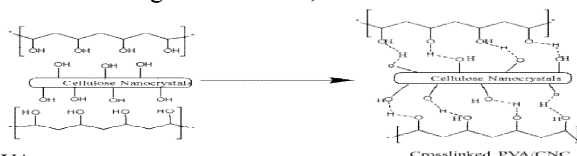


Fig.1. The mechanism of PVA crosslinking to CNCs.

\*Corresponding author: [asrk\\_saleh@yahoo.com](mailto:asrk_saleh@yahoo.com)

DOI: 10.21608/EJCHEM.2021.95020.4466

Receive Date: 08 September 2021, Revise Date: 05 October 2021, Accept Date: 13 October 2021

©2022 National Information and Documentation Center (NIDOC)

applications because of its hydrophilic properties, compatible chemical structure, flexibility, and high oxygen and barrier properties [11, 12].

PVA is an example of a man-made polymer that is made from an unrenovable and non-biodegradable sources [13, 14]. Due to its remarkable chemical and physical properties, including biocompatibility, temperature stability, and non-toxicity, it can be produced in large quantities, which allows it to be used as a surface material in a wide range of fields such as films [15, 16] and glue [17]. But given its semi-crystalline structure [18], low strength, and low thermal stability, it has been studied for various applications as a matrix of nanocomposites, but is often not used due to these disadvantages [19, 20].

Furthermore, CNC reinforcers also have the purpose of acting as a nucleating agent, as well as enhancing mechanical properties, such as tensile strength, Young's modulus, and storage modulus [21]. A promising alternative to antibiotics could be metallic nanoparticles (NPs) exhibiting antibacterial properties. Antibiotics with more specific mechanisms of action often have an advantage over those that affect different bacterial structures [22]. It is still unknown how NPs exert their antibacterial effects and the factors involved. Pure NPs can be improved by adding biological polymers (polyacrylonitrile, pyrrolidone, PVA, starch, gelatine, heparin, carboxymethylcellulose, and chitosan) and their stability can be increased [23-25]. Thermoplastic films used in packaging and/or the medical industry can be incorporated with nanomaterials, such as copper and silver, which act as antimicrobial materials. Copper nanoparticles are promising multifunctional antibacterial agents that have high biological activity, a low cost, and are ecologically safe [26]. Copper nanoparticles and copper-containing materials have demonstrated antibacterial properties in several studies [27]. Consequently, the development of antibacterial films using PVA/CNCs/Cu-NPs composites and evaluation of their antibacterial activity will result in the manufacture of new antibacterial composites. The aim of this study, embedding CNCs into PVA films, to improve their mechanical properties as well as test their antibacterial activity using Cu-NPs. The

antibacterial properties, structure, and morphology of the films were studied.

## 2. Experimental

### 2.1. Chemical compounds

The polymer PVA, a powder form (BDH chemical Ltd England) with a molecular weight of approximately 125,000 g/mol was used in the preparation of neat PVA and PVA/CNCs/Cu-NPs and PVA/CNCs films. We purchased copper (II) sulfate pentahydrate and sodium hydroxide NaOH from Sigma-Aldrich in India. No further purification was required for any of the other reagents or solvents used in this study.

### 2.2. Preparation of CNCs

The preparation of CNCs (Figure. 2) has been largely in line with the method described previously [28], utilizing hydrolysis with sulfuric acid to extract alpha-cellulose from rice husk. Twenty grams of rice husk pulp were combined with 200 ml of 64 weight percent sulfuric acids preheated to 45°C. After 25 minutes at 45°C, the reaction was diluted to 10 percent of its original concentration to stop it. A suspension was centrifuged for 15 minutes at 6,000 rpm followed by washing & centrifuging, again. The solution was dialyzed for several days to neutralize the remaining acid. Based on the gravimetric analysis, the concentration was 1.3 weight percent. Conduct metric titration was used to measure the surface charge, which was 0.6 mmol/g.

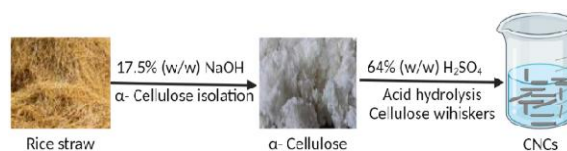


Fig. 2. Schematic of the stages of CNCs synthesis.

### 2.3. Synthesis of Cu-NPs

The Cu-NPs were synthesized by chemical reduction process using copper (II) sulfate pentahydrate as precursor salt and starch as capping agent as described by [29], with slight modification (Figure. 3). As part of the preparation procedure, 0.1 M copper (II) sulfate pentahydrate solution is added to 120 mL of starch (1.2%) solution with vigorous stirring for 30 minutes. After the synthesis solution was stirred rapidly under continuous stirring for 50 mL, 0.2 M hydroxylamine hydrochloride solution was added to it. After the solution was prepared, 30 ml of 1 M sodium hydroxide solution was slowly

added while stirring constantly and heated at 80°C for 2 hours.

As a result, the solution turned yellow. The solution was removed from the heat once the reaction had completed and allowed to settle overnight. To remove any remaining bound nanoparticles from the precipitates, they were washed three times with deionized water and ethanol after being separated from the solution by two successive centrifugation steps (1000 rpm). They were dried at room temperature after obtaining the yellow precipitates. We stored nanoparticles for further analysis in glass vials after drying.

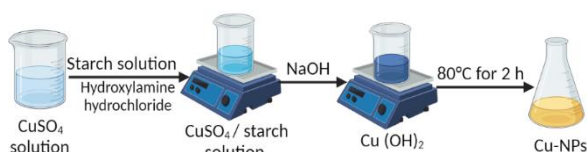


Fig. 3. Schematic of the stages of Cu-NPs synthesis

#### 2.4. Preparation of nanocomposite films

A solvent casting method was used to prepare PVA, PVA/CNCs, and PVA/CNCs/Cu-NPs films (Figure. 4). To prepare the PVA solution, it was added to 90 ml of water at 80°C for 4 h with constant stirring. PVA solution of 2g was poured into Teflon molds or glass Petri dishes (10 cm in diameter) and allowed to dry for 24 hours at room temperature. Using an ultra turrax homogenizer, CNCs were homogenized at 4000 rpm for 15 minutes before being sonicated for 10 minutes at room temperature. The procedure for producing PVA/CNCs films is the same as that for pure PVA films. Several nanocellulose loadings were used in the preparation of PVA/CNCs films. In the meantime, CNC suspensions (2.5, 5, 7.5, and 10% between PVA and CNCs) were continuously stirred at 80°C for three hours. Also by the same procedure, PVA films containing 7.5 wt % CNCs and various levels of Cu-NPs (1, 2, 4, and 8 wt % based on CNCs) were prepared. A vacuum dryer was used to remove the remaining solvent (chloroform) from all prepared films after they had dried at room temperature for 24 h

#### 2.5. Characterization of prepared nanocomposites films

##### 2.5.1. Transmission electron microscopy (TEM)

The morphology and particle size of the CNCs and Cu-NPs were characterized using TEM (JEOL, JEM-1230 electron microscope) at an operating voltage of 76 kV.

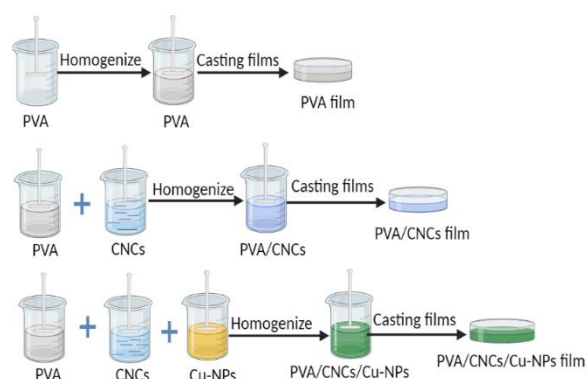


Fig. 4. Schematic of the stages of PVA/CNCs/Cu-NPs film synthesis.

##### 2.5.2. XRD analysis

The XRD patterns of the prepared films were carried out on a Diano X-ray diffractometer using a Cu ( $K\alpha_1/K\alpha_2$ ) radiation source energized at 45 kV and a Philips X-ray diffractometer (PW 1930 generator, PW 1820 goniometer). The XRD patterns were recorded in a diffraction angle range from  $\theta = 10^\circ$  to  $80^\circ$ .

##### 2.5.3. Fourier transform infrared (FT-IR) spectral analysis

FT-IR spectra of the prepared CNCs were recorded in the range of 400–4000  $\text{cm}^{-1}$  using Shimadzu 8400S FT-IR Spectrophotometer.

##### 2.5.4. SEM analysis

The surface morphology of the prepared nanocomposites films was analyzed using SEM, (JSM 6360LV, JEOL/Noran). The microscope was attached to a dispersive energy spectrometer. The samples were coated with a thin layer of gold using a fine coater (JEOL –JFC 1200 FINE COATER) before the examination. The images were obtained using an accelerating voltage of 10–15 kV.

##### 2.5.5. TGA and DTA analysis

To measure the thermal stability and differential thermal properties of the nanocomposites films, a TGA (Shimadzu DTG-60), Japan, was used. At room temperature, samples were heated to 800°C under an oxygen atmosphere at a rate of 10°C/min.

##### 2.5.5. Mechanical properties

The tensile test was performed with a Lloyd Instrument (Lloyd Instruments, West Sussex, United Kingdom) and a 100-N load cell. The crosshead speed was set at 2 mm/min at 25°C during the measurements.

### 2.6. Assay of antibacterial activity

The model bacteria used, *Escherichia coli* (ATCC 25922) (*E. coli*) and *Pseudomonas aeruginosa* (ATCC 27853) (*P. aeruginosa*) as Gram-negative, *Bacillus subtilis* (*B. subtilis*) and *Staphylococcus aureus* (ATCC 25923) (*S. aureus*) as Gram-positive bacteria were maintained on Luria–Bertani (LB) agar medium at 4°C. The antibacterial activity of the prepared nanocomposite films (PVA, PVA/CNCs and PVA/CNCs/Cu-NPs) at different concentrations was investigated by disk diffusion technique and the film of PVA only were used as a control [30, 31]. Briefly, LB medium composed of (g/l): peptone 10, yeast extract 5, sodium chloride 5 and agar 20 and medium pH was adjusted to 7 and autoclaved at 121°C for 20 min [32]. The model bacteria were cultured and spread (optical density at 600 nm reached 0.2.) on agar plates. Over this inoculated medium, the dry disks of nanocomposite films (5mm) were placed and incubated for 24 h at 37°C. The nanocomposites films were sterilized by ultraviolet (UV) for 30 min [33]. The antibacterial activity of films was photographed and determined by measuring the diameter of the inhibition zone. Triplicate experiments were done for each film and the average values were recorded.

## 3. Results and discussion

### 3.1. Characterization of the prepared nanocomposites films

Figure 5 illustrates how CNCs are prepared. As illustrated in Figure 5(A), the width of CNCs isolated from rice husk falls between 4 and 8 nm, while the length was between 80 and 170 nm [34–36]. The XRD pattern of the CNCs revealed the crystalline peaks at  $2\theta = 16$  and  $22$  associated with the cellulose I diffraction peaks. Figure 5(B) shows that these peaks correlate with reflection from the 110 and 200 planes of cellulose I, respectively. A crystallinity index of about 82 % was calculated for the CNCs [37]. According to FTIR evaluations of CNCs, a wide peak at  $3420\text{ cm}^{-1}$  corresponds to O-H stretching vibration, peak at  $2924\text{ cm}^{-1}$  pertains to

O-H stretching and C-H stretching vibrations. On the other hand, the peak at  $1630\text{ cm}^{-1}$  is ascribed to water molecules adsorbed on the surface of CNCs. The peaks correspond to the stretching vibration of C-O for glycosidic bonds and C-O of primary and secondary hydroxyl groups, as well as an out-of-plane deformational vibration for O-H groups as shown in Figure 5(C).

A TEM analysis showed that the synthesized Cu particles are approximately spherical in shape and their size ranges between 28–36 nm. The size and shape of the synthesized Cu particles were determined by TEM as shown in Figure 6.

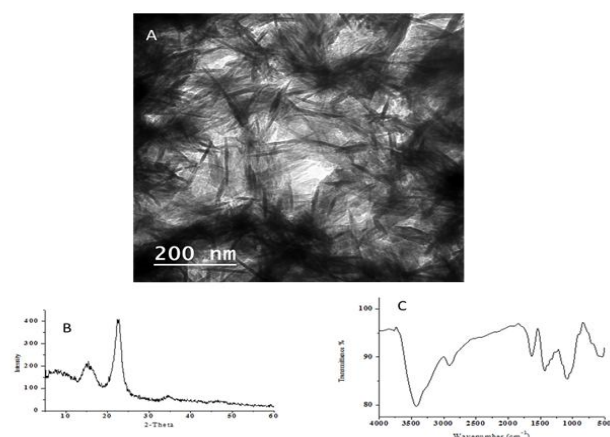


Fig. 5. A is TEM, B is FTIR and C is XRD of CNCs.

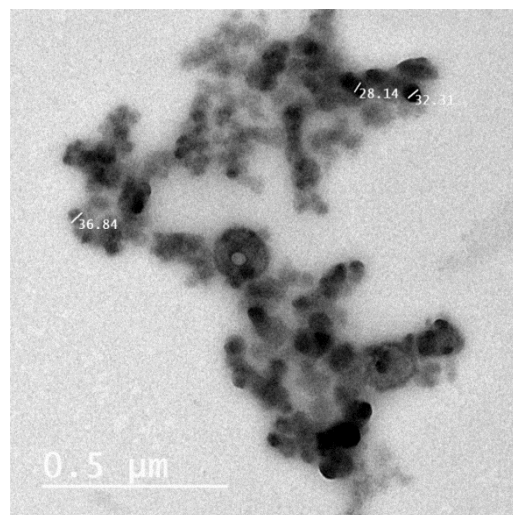


Fig. 6. TEM image of the prepared Cu-NPs.

To determine the surface morphology of prepared nanocomposites films, the SEM was applied as showed in Figure 7, the surface roughness of the

films was enhanced by loading them with CNCs and Cu-NPs while the surface roughness of the films was uniform for neat PVA films. A high density of Cu-NPs is observed on the surface compared with the images in Figure. 7(c) which may arise from the aggregation of smaller size Cu-NPs, while Figure. 7(b) shows a low density of CNCs aggregation on the surface of the PVA film, the CNCs and Cu-NPs loaded with Cu showed very small amounts of Cu. Crystallinity was analyzed for the films made from nanocomposites.

XRD patterns of PVA, PVA/CNCs and PVA/CNCs/Cu-NPs are illustrated in Figure. 8. It can be observed from the XRD of pure PVA film that a broad peak is detected in Figure 8a at about  $2\theta$  angle of  $20.00^\circ$  for PVA film without additions confirms the semi-crystalline arrangement [38], and refer to 101 reflection planes. The source for this structure is the interaction between the molecules inside the PVA chains through H-bonding. Two broad peaks of lower intensity at about  $2\theta$  angles of 8 and 12 are observed, these peaks indicate the presence of the CNCs [34]. The individual nanoparticles of Cu appear at  $2\theta = 30, 37$  are observed for XRD patterns of PVA/CNCs/Cu-NPs films. The PVA film loaded by 7.5% CNCs and 8% Cu-NPs has higher crystallinity than that of either pure PVA film or PVA/CNCs only. This may be attributed to the physically binding effect of Cu-NPs that could make alignment of the CNCs resulting in enhancement of crystalline regions. XRD analysis of pure PVA, PVA/CNCs and PVA/CNCs/Cu-NPs nanocomposites films revealed the major change in the structure and morphology of the nanocomposites by addition of CNCs and Cu-NPs. In each case, there is a transition to a more crystalline structure by the addition of CNCs and CNCs/Cu-NPs as shown in SEM images.

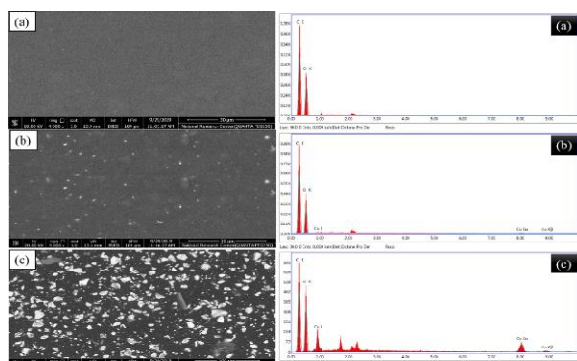


Fig. 7. SEM and EDX for neat PVA (a), PVA/CNCs (b), and PVA/CNCs/Cu-NPs (c) nanocomposites films.

Table 1. Chemical compositions obtained from EDX for PVA, PVA/CNCs, and PVA/CNCs/Cu-NPs nanocomposites films

| Sample          | Element | Weight % | Atomic % | Net Int. | Error % |
|-----------------|---------|----------|----------|----------|---------|
| PVA             | CK      | 56.13    | 63.02    | 167.02   | 6.25    |
|                 | OK      | 43.87    | 36.98    | 85.88    | 11.42   |
| PVA/CNCs        | CK      | 57.91    | 65.12    | 153.2    | 6.37    |
|                 | OK      | 41.06    | 34.66    | 69.56    | 11.73   |
| PVA/CNCs/Cu-NPs | CK      | 49.03    | 60.95    | 112.08   | 8.25    |
|                 | OK      | 38.76    | 36.18    | 85.17    | 11.27   |
|                 | CuK     | 12.21    | 2.87     | 30.59    | 8.56    |

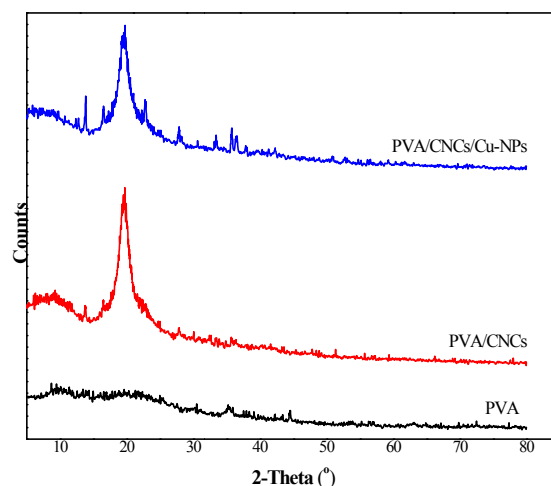


Fig. 8. XRD patterns of pure PVA, PVA/CNCs and PVA/CNCs/Cu-NPs nanocomposites films.

In Figure. 9 and Figure. 9(a), all four nanocomposite films showed four distinct weight loss steps. Figure. 9 shows the TGA and DTA curves for PVA, PVA/CNCs, and PVA/CNCs/Cu-NPs. In the first step, the humidity would be removed (and weakly physically adsorbed water would be reduced). The second step at  $210\text{--}250^\circ\text{C}$  (decomposition of CNCs- Cu-NPs nanocomposites). The third step occurs between  $230$  and  $330^\circ\text{C}$  (decomposition of the side chains in PVA), and the last step occurs between  $330$  and  $500^\circ\text{C}$  (decomposition of the main chains in

PVA). In every film sample, a large amount of weight loss was observed between 210°C to 500°C, which corresponds to the maximum structural degradation of PVA at the temperature corresponding to the maximum weight loss and decomposition rate. This is illustrated in Figure. 9(b), where we see that the  $T_{max}$  of PVA/CNCs/Cu-NPs nanocomposite film has shifted up from 255 to 277 and 285°C, as opposed to PVA and PVA/CNCs films. As a result of the Cu-NPs embedded in the PVA matrix, the PVA/Cu-NPs films exhibited a slight shift toward high temperatures, indicating that the composite films typically had higher thermal stability.

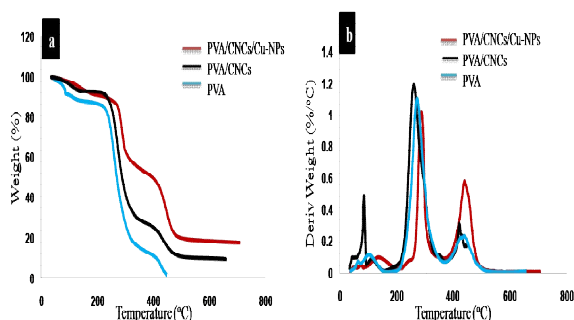


Fig. 9. Thermogravimetric analysis (a-TGA) and (b-DTA) of PVA Film, PVA film loaded by 7.5 wt% CNCs, PVA film loaded by 7.5 wt% CNCs and Cu-NPs.

The data represented in Figure. 10 (a and b) revealed that the PVA film reinforced with CNCs and Cu-NPs is mechanically stronger and tougher than the pure PVA film. This may be attributed to the nanocrystalline character of the films and the better interfacial adhesion between the PVA matrix and fibers and their very high surface area in addition to their homogeneous distribution in PVA films as well as the presence of Cu-NPs embedded in the PVA matrix. The decrease in tensile strength above 7.5% CNC could be due to the potential aggregation of CNCs. Tensile strength values were found to be 40.83, 45.68, 53.84, 61.84, and 54.5 MPa on varying the amount of CNCs from zero to 2.5, 5.0, 7.5 and 10%, respectively. The addition of CNCs resulted in a remarkable increase of its tensile strength up to nanocrystals loading of 7.5%, above which a decrease in tensile strength took place. The Tensile strength values increased from 61.84 for PVA film loaded by 7.5% CNCs to be 83.01, 102.85, 120.53 and 93.33 for PVA films loaded by 7.5% CNCs and 1, 2, 4 and 8% Cu-NPs, respectively in presence of

by 7.5% CNCs. The mechanical testing shows that the tensile strength increases with the increase in the percentage of CNCs or Cu-NPs and the vice versa for the Young's Modulus. As shown in Figure. 11 (a and b), pure PVA films have Young's Modulus higher than that of films loaded by CNCs or CNCs/Cu-NPs. Young's Modulus is progressively reduced with an increase of the CNCs or Cu-NPs content. This may be attributed to the low elasticity of the films and large deformations of the PVA matrix resulted from the potential aggregation of either

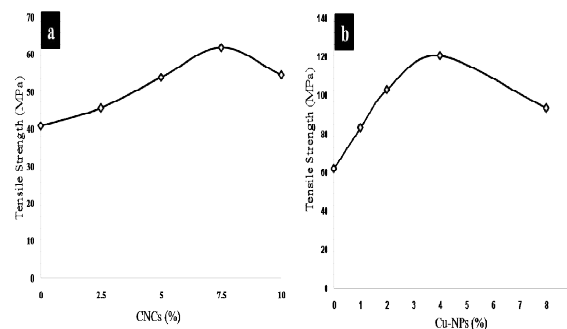


Fig. 10. Tensile strength of PVA at different concentrations of CNCs (a) and PVA/CNCs at different concentrations of Cu-NPs (b).

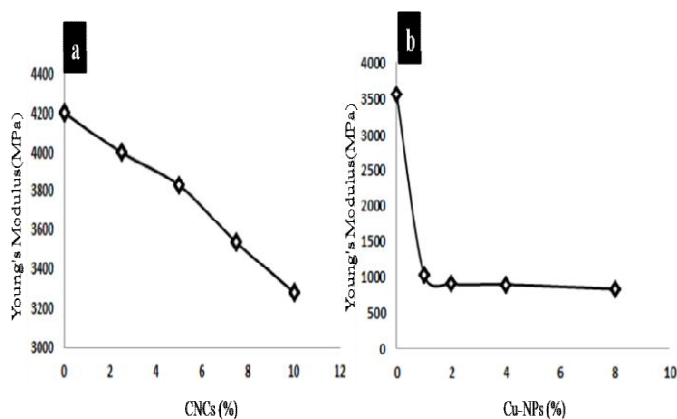


Fig. 11. Young's Modulus of PVA at different concentrations of CNCs (a) and PVA/CNCs at different concentrations of Cu-NPs (b).

### 3.2. Antibacterial evaluation

In the food packaging film industry, antibacterial activity is one of the most important parameters. In the study, nanocomposites films with and without Cu-NPs were evaluated at various concentrations for their antibacterial effects against model bacteria. According to the diameters of inhibition zones in Figure. 12 and Table 2, both *B subtilis* and *S aureus*

were found to possess higher antibacterial activities as Gram-positive bacteria followed by *P. aeruginosa* and *E. coli* as Gram-negative bacteria. In accordance with other studies [39], the antibacterial activity of the nanocomposites films increased as the concentration of Cu-NPs increased. On the other hand, *E. coli* showed less antibacterial activity. Furthermore, as shown in Figure. 12, although 10% of the PVA and PVA/CNC films did not reveal antibacterial activity when used in CNCs. It is still unclear how Cu-NPs exert their antibacterial effect, but their antimicrobial activity can be explained by the electrostatic attraction between cell membranes and Cu ions.

Due to the concentration of Cu ions, damage to the cell membrane can occur. Free radicals formed from the surface of the Cu-NPs cause damage to the bacterial cells, in the same way as silver ions [40]. Cu nanocomposite films have shown antibacterial activity similar to Ag ions, which is attributed to the release of ions and the formation of reactive oxygen species [41, 42]. There are three most accepted and reported mechanisms by which metallic nanostructures exert their biocidal activity, but none is fully understood and accepted. (1) accumulation and dissolution of NPs in the membrane of bacteria alters membrane permeability, leading to the release of lipopolysaccharides, membrane proteins, and intracellular biomolecules and dissipation of the proton motive force across the plasma membrane. (2) generation of reactive oxygen species (ROSs) or/and their corresponding ions from NPs, following which cellular structures are damaged by oxidative stress; and (3) uptake of metallic ions derived from NPs or of NPs as a whole into cells, followed by depletion of intracellular ATP production and disruption of DNA replication [43].

#### 4. Conclusion

In this work, nanocomposites films, PVA loaded by CNCs prepared from rice husk and PVA loaded by CNCs and copper nanoparticles (Cu-NPs) fabricated by solution casting, were successfully prepared. The physical properties of the films were characterized by different techniques. The results showed a noticeable improvement of in the mechanical and thermal properties of the blend films. Also, the results showed that PVA/CNCs/Cu-NPs films have efficient antibacterial activity against

Gram-negative and Gram-positive strains and are promising to be used as packaging material.

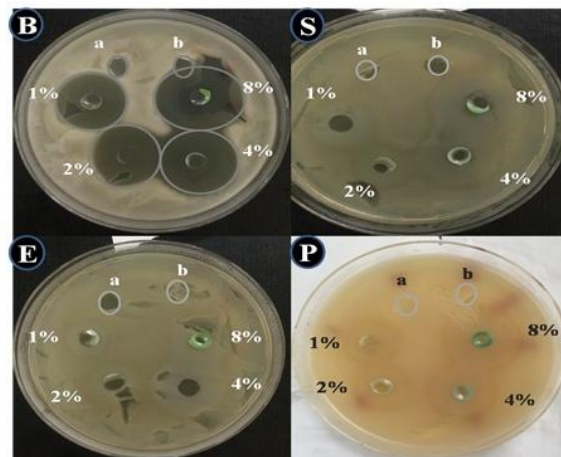


Fig. 12. Optical images of inhibition zones of PVA, PVA/CNCs and PVA/CNCs/Cu-NPs nanocomposites films: *B. subtilis* (B), *S. aureus* (S), *E. coli* (E) and *P. aeruginosa* (P). In all plates, (a) PVA/CNCs, (b) PVA, while other samples are PVA/CNCs incorporated with 1 to 8% of Cu-NPs.

Table 2. Diameter of inhibition zone of PVA/CNCs nanocomposites films at different concentrations from Cu-NPs.

| Organism            | Diameters of inhibition zone (mm)  |    |    |    |
|---------------------|------------------------------------|----|----|----|
|                     | Different concentrations of Cu-NPs |    |    |    |
|                     | 1%                                 | 2% | 4% | 8% |
| <i>E. coli</i>      | 21                                 | 23 | 24 | 21 |
| <i>P. aeruginos</i> | 22                                 | 23 | 25 | 29 |
| <i>a</i>            |                                    |    |    |    |
| <i>B. subtilis</i>  | 25                                 | 26 | 29 | 33 |
| <i>S. aureus</i>    | 23                                 | 24 | 26 | 30 |

#### 5. Declarations

Conflict of interest, the authors declare that they have no known competing financial interests or personal relationships that could have appeared to influence the work reported in this paper.

#### 6. CRediT Authorship contributions statement

**Ahmed El-Gendy:** Conceptualization, Resources, Review & editing, Project administration, **Mohamed A. Diab:** Methodology, Investigation, Formal analysis, Experimental details, Writing-original draft, **Ragab E. Abou-Zeid:** Methodology, Investigation,

Formal analysis, Experimental details, Writing & editing, **Ahmed K. Saleh**: Methodology, Investigation, Experimental details, Writing –review & editing.

## 7. Acknowledgement

The authors acknowledge the financial support by the National Research Centre, Cairo, Egypt, project number P100107.

## 9. References

- [1] C.B. Field, J.E. Campbell, D.B. Lobell, Biomass energy: the scale of the potential resource, *Trends Ecol. Evol.* 23(2) (2008) 65-72.
- [2] L. Xie, M. Liu, B. Ni, X. Zhang, Y. Wang, Slow-release nitrogen and boron fertilizer from a functional superabsorbent formulation based on wheat straw and attapulgite, *Chem. Eng. J.* 167(1) (2011) 342-348.
- [3] B.L. Peng, N. Dhar, H. Liu, K. Tam, Chemistry and applications of nanocrystalline cellulose and its derivatives: a nanotechnology perspective, *The Canadian journal of chemical engineering* 89(5) (2011) 1191-1206.
- [4] S.Y. Ooi, I. Ahmad, M.C.I.M. Amin, Cellulose nanocrystals extracted from rice husks as a reinforcing material in gelatin hydrogels for use in controlled drug delivery systems, *Industrial Crops and Products* 93 (2016) 227-234.
- [5] K. Nagarajan, N. Ramanujam, M. Sanjay, S. Siengchin, B. Surya Rajan, K. Sathick Basha, P. Madhu, G. Raghav, A comprehensive review on cellulose nanocrystals and cellulose nanofibers: Pretreatment, preparation, and characterization, *Polymer Composites* 42(4) (2021) 1588-1630.
- [6] N. Grishkewich, N. Mohammed, J. Tang, K.C. Tam, Recent advances in the application of cellulose nanocrystals, *Current Opinion in Colloid & Interface Science* 29 (2017) 32-45.
- [7] D. Trache, M.H. Hussin, M.M. Haafiz, V.K. Thakur, Recent progress in cellulose nanocrystals: sources and production, *Nanoscale* 9(5) (2017) 1763-1786.
- [8] R.E. Abou-Zeid, M.A. Diab, S.A. Mohamed, A. Salama, H.A. Aljohani, K.R. Shouair, Surfactant-assisted poly (lactic acid)/cellulose nanocrystal bionanocomposite for potential application in paper coating, *Journal of Renewable Materials* 6(4) (2018) 394-401.
- [9] S. Yenidoğan, Nanocrystalline Cellulose and Polyvinyl Alcohol Coating Application to Cardboard Packaging Papers and Investigation of the Effects on Paper Properties, *Materials Science* 26(3) (2020) 317-322.
- [10] B. Xing, X. Xu, W. Hu, R. Ni, Y. Zhao, Highly Thermal Resistant and Biodegradable Textile Sizes from Glycols Modified Soy Proteins for Remediation of Textile Effluents, *Macromolecular Materials and Engineering* 306(4) (2021) 2000751.
- [11] P. Zhang, K. Wang, J. Wang, J. Guo, S. Hu, Y. Ling, Mechanical properties and prediction of fracture parameters of geopolymer/alkali-activated mortar modified with PVA fiber and nano-SiO<sub>2</sub>, *Ceramics International* 46(12) (2020) 20027-20037.
- [12] N. Limpan, T. Prodpran, S. Benjakul, S. Prasarpran, Influences of degree of hydrolysis and molecular weight of poly (vinyl alcohol)(PVA) on properties of fish myofibrillar protein/PVA blend films, *Food Hydrocoll* 29(1) (2012) 226-233.
- [13] E.-R. Kenawy, E.A. Kamoun, M.S.M. Eldin, M.A. El-Meligy, Physically crosslinked poly (vinyl alcohol)-hydroxyethyl starch blend hydrogel membranes: Synthesis and characterization for biomedical applications, *Arabian Journal of Chemistry* 7(3) (2014) 372-380.
- [14] E.A. Kamoun, X. Chen, M.S.M. Eldin, E.-R.S. Kenawy, Crosslinked poly (vinyl alcohol) hydrogels for wound dressing applications: A review of remarkably blended polymers, *Arabian Journal of chemistry* 8(1) (2015) 1-14.
- [15] A. Jayakumar, K. Heera, T. Sumi, M. Joseph, S. Mathew, G. Praveen, I.C. Nair, E. Radhakrishnan, Starch-PVA composite films with zinc-oxide nanoparticles and phytochemicals as intelligent pH sensing wraps for food packaging application, *Int J Bio Macromol* 136 (2019) 395-403.
- [16] A. Karimi, M. Navidbakhsh, Mechanical properties of PVA material for tissue engineering applications, *Materials technology* 29(2) (2014) 90-100.
- [17] M.M. Silva, T.A.B.C. Sanjad, M.L.d. Costa, S.d.P.S.E. Costa, Lime-based restoration paints: characterization and evaluation of formulations using a native species from the Amazon flora and PVA-based glue as additives, *Ambiente Construído* 17(3) (2017) 7-23.
- [18] D. Thomas, P. Cebe, Self-nucleation and crystallization of polyvinyl alcohol, *Journal of Thermal Analysis and Calorimetry* 127(1) (2017) 885-894.

- [19] H. Lee, R. Mensire, R.E. Cohen, M.F. Rubner, Strategies for hydrogen bonding based layer-by-layer assembly of poly (vinyl alcohol) with weak polyacids, *Macromolecules* 45(1) (2012) 347-355.
- [20] D. Han, L. Yan, W. Chen, W. Li, Preparation of chitosan/graphene oxide composite film with enhanced mechanical strength in the wet state, *Carbohydr Polym* 83(2) (2011) 653-658.
- [21] T.S. Gaaz, A.B. Sulong, M.N. Akhtar, A.A.H. Kadhum, A.B. Mohamad, A.A. Al-Amiery, Properties and applications of polyvinyl alcohol, halloysite nanotubes and their nanocomposites, *Molecules* 20(12) (2015) 22833-22847.
- [22] K. Kon, M. Rai, Metallic nanoparticles: mechanism of antibacterial action and influencing factors, *J Comp Clin Path Res* 2(2) (2013) 160-174.
- [23] A. Sathiyaseelan, K. Saravanakumar, A.V.A. Mariadoss, M.-H. Wang, Antimicrobial and Wound Healing Properties of FeO Fabricated Chitosan/PVA Nanocomposite Sponge, *Antibiotics* 10(5) (2021) 524.
- [24] M. Hashmi, S. Ullah, I.S. Kim, Copper oxide (CuO) loaded polyacrylonitrile (PAN) nanofiber membranes for antimicrobial breath mask applications, *Current Research in Biotechnology* 1 (2019) 1-10.
- [25] W. Li, Y. Yang, H. Zhang, Z. Xu, L. Zhao, J. Wang, Y. Qiu, B. Liu, Improvements on biological and antimicrobial properties of titanium modified by AgNPs-loaded chitosan-heparin polyelectrolyte multilayers, *J. Mater. Sci. Mater. Med.* 30(5) (2019) 1-12.
- [26] M. Kargar, H. Ahari, S. Kakoolaki, M. Mizani, Synthesis of Nano silver and copper by chemical reduction method to produce of NanoTiO<sub>2</sub> composites (based on Ag & copper) antimicrobial nano-coated packaging to increase the shelf life of caviar (Huso huso fish fillets), *Iran. J. Fish. Sci.* 20(1) (2021) 13-31.
- [27] T.S.M. Kumar, M. Chandrasekar, K. Senthilkumar, R. Ilyas, S. Sapuan, N. Hariram, A.V. Rajulu, N. Rajini, S. Siengchin, Characterization, thermal and antimicrobial properties of hybrid cellulose nanocomposite films with in-situ generated copper nanoparticles in Tamarindus indica Nut Powder, *J Polym Environ* 29(4) (2021) 1134-1142.
- [28] N.A. El-Wakil, E.A. Hassan, R.E. Abou-Zeid, A. Dufresne, Development of wheat gluten/nanocellulose/titanium dioxide nanocomposites for active food packaging, *Carbohydrate polymers* 124 (2015) 337-346.
- [29] H. Abou-Yousef, E. Saber, M.S. Abdel-Aziz, S. Kamel, Efficient alternative of antimicrobial nanocomposites based on cellulose acetate/Cu-NPs, *Soft Materials* 16(3) (2018) 141-150.
- [30] S. Ebrahimiasl, A. Rajabpour, Synthesis and characterization of novel bactericidal Cu/HPMC BNCs using chemical reduction method for food packaging, *Journal of food science and technology* 52(9) (2015) 5982-5988.
- [31] A. Manikandan, M. Sathiyabama, Green synthesis of copper-chitosan nanoparticles and study of its antibacterial activity, *Journal of Nanomedicine & Nanotechnology* 6(1) (2015) 1.
- [32] R. Yahia, M.E. Owda, R.E. Abou-Zeid, F. Abdelhai, E.S. Gad, A.K. Saleh, H.Y. El-Gamil, Synthesis and characterization of thermoplastic starch/PVA/cardanol oil composites loaded with in-situ silver nanoparticles, *J. Appl. Polym. Sci.* (2021) 51511.
- [33] R. Li, M. He, T. Li, L. Zhang, Preparation and properties of cellulose/silver nanocomposite fibers, *Carbohydr Polym* 115 (2015) 269-275.
- [34] R.E. Abou-Zeid, E.A. Hassan, F. Bettaieb, R. Khiari, M.L. Hassan, Use of cellulose and oxidized cellulose nanocrystals from olive stones in chitosan bionanocomposites, *Journal of Nanomaterials* 2015 (2015).
- [35] M.L. Hassan, R.E. Abou-Zeid, S.M. Fadel, M. El-Sakhawy, R. Khiari, Cellulose nanocrystals and carboxymethyl cellulose from olive stones and their use to improve paper sheets properties, *International Journal of Nanoparticles* 7(3-4) (2014) 261-277.
- [36] G. Siqueira, J. Bras, A. Dufresne, Cellulosic bionanocomposites: a review of preparation, properties and applications, *Polymers* 2(4) (2010) 728-765.
- [37] P. Zugenmaier, Conformation and packing of various crystalline cellulose fibers, *Prog. Polym. Sci.* 26(9) (2001) 1341-1417.
- [38] N. Rithin Kumar, V. Crasta, R.F. Bhajantri, B. Praveen, Microstructural and mechanical studies of PVA doped with ZnO and WO<sub>3</sub> composites films, *Journal of Polymers* 2014 (2014).
- [39] T. Zhong, G.S. Oporto, J. Jaczynski, C. Jiang, Nanofibrillated cellulose and copper nanoparticles embedded in polyvinyl alcohol films for antimicrobial applications, *BioMed research international* 2015 (2015).
- [40] C. Triebel, S. Vasylyev, C. Damm, H. Stara, C. Özpınar, S. Hausmann, W. Peukert, H. Münstedt, Polyurethane/silver-nanocomposites with enhanced silver ion release using

- 
- multifunctional invertible polyesters, *Journal of Materials Chemistry* 21(12) (2011) 4377-4383.
- [41] M.J. Hajipour, K.M. Fromm, A.A. Ashkarran, D.J. de Aberasturi, I.R. de Larramendi, T. Rojo, V. Serpooshan, W.J. Parak, M. Mahmoudi, Antibacterial properties of nanoparticles, *Trends Biotechnol.* 30(10) (2012) 499-511.
- [42] J.R. Morones, J.L. Elechiguerra, A. Camacho, K. Holt, J.B. Kouri, J.T. Ramirez, M.J. Yacaman, The bactericidal effect of silver nanoparticles, *Nanotechnology* 16(10) (2005) 2346.
- [43] A.K. Chatterjee, R. Chakraborty, T. Basu, Mechanism of antibacterial activity of copper nanoparticles, *Nanotechnology* 25(13) (2014) 135101.